Ionic Liquid Droplet Micro-Reactor for Catalysis Reactions not at Equilibrium

Ming Zhang,[†] Rammile Ettelaie,[#] Tao Yan,[†] Suojiang Zhang,[‡] Fangqin Cheng,[⊥] Bernard P. Binks,[§] and Hengquan Yang*,[†]

[†] School of Chemistry and Chemical Engineering, Shanxi University, Taiyuan 030006, China

[#] Food Colloids Group, School of Food Science and Nutrition, University of Leeds, Leeds LS2 9JT, U.K.

[‡] Beijing Key Laboratory of Ionic Liquids Clean Process, Key Laboratory of Green Process and Engineering, Institute of Process Engineering, Chinese Academy of Sciences, Beijing 100190, China.

[⊥] Institute of Resources and Environment Engineering, Shanxi University, Taiyuan 030006, China

[§] School of Mathematics and Physical Sciences, University of Hull, Hull. HU6 7RX. U.K.

Supporting Information

ABSTRACT: We develop a novel strategy to more effectively and controllably process continuous enzymatic or homogeneous catalysis reactions based on non-aqueous Pickering emulsions. A key element of this strategy is "bottom-up" construction of a macroscale continuous flow reaction system through packing catalyst-containing micron-sized ionic liquid (IL) droplets in oil in a column reactor. Due to the continuous influx of reactants into the droplets and the continuous release of products from the droplets, catalysis reactions in such a system can take place without limitations arising from establishment of the reaction equilibrium and catalyst separation, inherent in conventional batch reactions. As proof of the concept, enzymatic enantioselective trans-esterification and CuI-catalyzed cycloaddition reactions using this IL droplet-based flow system both exhibit eight to twenty-fold enhancement in catalysis efficiency compared to their batch counterparts, and a durability of at least 4000 h for the enantioselective trans-esterification of 1-phenylethyl alcohol, otherwise unattainable in their batch counterparts. We further establish a theoretical model for such a catalysis system working under non-equilibrium conditions, which not only supports the experimental results but also helps to predict reaction progress at a microscale level. Being operationally simple, efficient and adaptive, this strategy provides an unprecedented platform for practical applications of enzymes and homogeneous catalysts even at a controllable level.

1. INTRODUCTION

Homogeneous catalysis and enzymatic reactions are widely used in laboratory synthesis and even in large-scale fabrication of various chemicals.[1–3] Most of these reactions have to be carried out in a batch manner because they require separation of products from catalysts at the end of reaction.[1,4,5] However, batch reactions often suffer from the limitation of reaction equilibrium[2,6] and their inability for the continuous use of the catalyst.[1,7] Although a few homogenous catalysis and enzymatic reactions can be carried out in continuously stirred tank reactors (CSTR), this still hardly overcomes the limitation of reaction equilibrium[8] and is incapable of continuously using the enzymes and homogenous catalysts.[9,10] Furthermore, the batch reaction is sometimes limited by the product inhibition effect especially in many enzymatic reactions, leading to

a low level of conversion.[2,11–14] Moreover, batch reactions are often carried out in a bulk liquid phase, where mass transport and heat transfer have to rely on external mechanical agitation.[15,16] Such a "top-down" method for homogenizing macroscale reaction systems using agitation is incompetent for the precise control of local reactions due to the lack of homogeneity at a microscale level,[15,17–19] especially for multiphase reactions involving viscous liquids, leading to difficulty in scale-up.

Reactions involving liquid droplets including microfluidic platforms[20–27] and Pickering emulsions[28–33] have demonstrated that droplet micro-reactors potentially allow the control of multiphase reactions on a microscale even without the need for agitation and continuous reaction.[34] However, microfluidic systems are unable to immobilize the droplets, and thus cannot tackle the long-standing issues such as the product inhibition effect and the
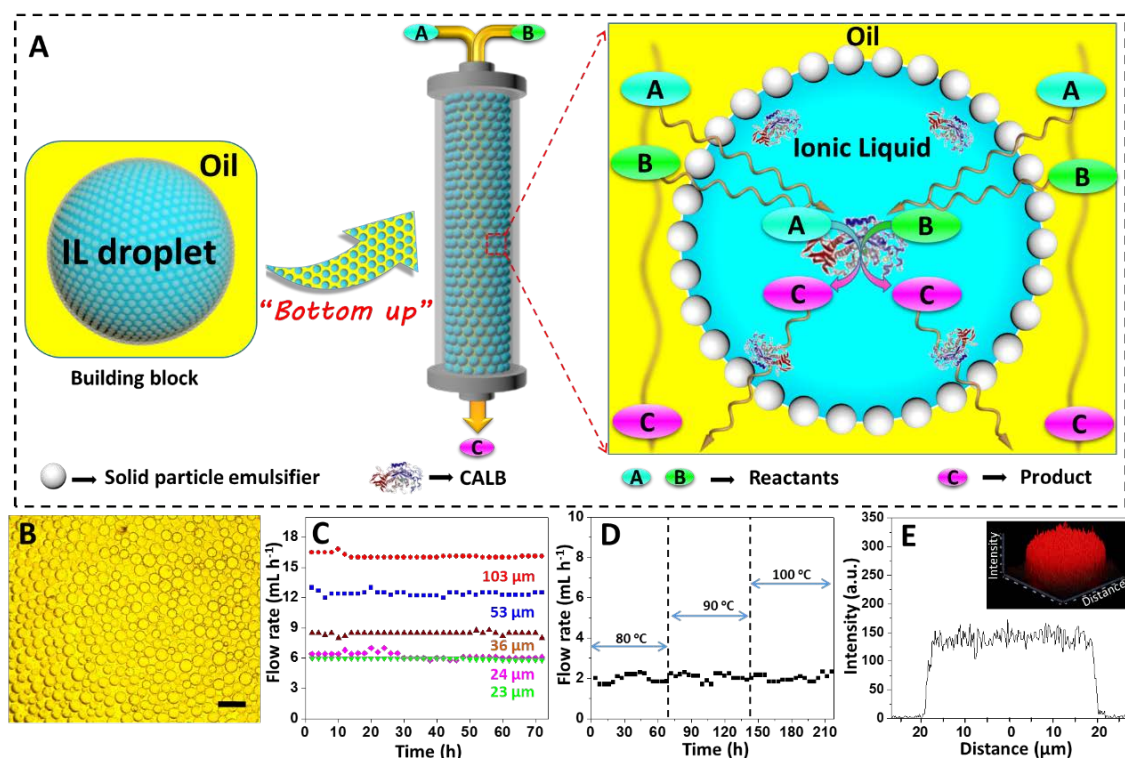
Figure 1. IL droplet-based continuous flow catalysis system. (A) Schematic illustration of construction of a continuous flow catalysis system using ionic liquid (IL) droplets in oil as building blocks. (B) Optical microscopy image of particle-stabilized IL droplets in oil, scale bar = 100 μm. (C) Flow rate of the oil as a function of IL droplet size (column diameter is 2 cm and the emulsions consist of 6.5 g of [BMIM]PF$_6$, 2.4 mL of *n*-octane and particle emulsifier at 1, 2, 3, 4 or 5 wt % (with respect to the ionic liquid)). (D) Thermal stability of the IL droplets under the oil-flowing conditions at 80, 90 and 100 °C, flow rate = 2 mL h^{-1}. (E) 3D confocal fluorescence microscopy for the distribution of Rhodamine B-labeled enzyme within an IL droplet and its fluorescence intensity profile along its diameter. The IL-in-oil emulsions are all formulated with [BMIM]PF$_6$, *n*-octane and 3 wt % particle emulsifier except for that in Figure 1C.

separation/recycling of homogeneous catalysts.[21] Recently, our group has developed a Pickering emulsion strategy, in which droplets are stabilized by particles, to continuously process aqueous biphasic catalysis reactions.[34] At the same time, this droplet-based strategy also overcomes some disadvantages associated with batch reactions such as the need for agitation and the separation of catalysts from the reaction medium. Nevertheless, in this system, catalysis reactions occur only at the interfaces of water droplets in oil rather than within the droplets, and the catalysts inside droplets are not accessible to reactant molecules because organic reactants are mostly insoluble in water. Moreover, this water-oil reaction system is obviously unable to realize efficient control over reactions at a microscale level because the reaction occurrence is still uniform on the length scale of a droplet. Furthermore, it is also not particularly suitable to water-sensitive reactions.

Herein, to continuously process enzymatic or homogeneous catalysis reactions more efficiently and more controllably even at a microscale level, we develop a non-aqueous continuous flow system that allow reactions to take place within the droplets. This system adopts catalyst-containing micron-sized ionic liquid (IL)

droplets in an immiscible oil as building blocks to construct a macroscale flow reaction by packing these IL-based emulsion droplets in a column reactor, in a "bottom-up" fashion, as schematically illustrated in Figure 1A. In this scenario, the IL droplet movement is restricted because of the packing effect, while the oil phase outside the IL droplets (continuous phase) and reactants dissolving in it can percolate through the packed droplet network due to gravity or applied pressure. Owing to a dissolution effect, a continuous influx of reactants from the continuous phase into the IL droplets and a steady release of products from the droplets to the continuous phase, catalysis reactions can proceed under non- equilibrium steady conditions although the reaction equilibrium is not altered (maintaining the reaction always away from the equilibrium).[35–37] Consequently, the catalysis efficiency is significantly boosted and is well maintained even after a period of 4000 h, which is demonstrated here by the enzymatic enantioselective trans-esterification and the CuI-catalyzed azide–alkyne cycloaddition. The key principles for such a catalysis system are also established theoretically in the current work.

2. RESULTS AND DISCUSSION

2.1. Design and Preparation of IL Droplet Micro-Reactors. We chose ionic liquids (ILs) to make up the droplet micro-reactors to mimic artificial chemical cells, based on the following considerations: (i) They are not only considered as environmentally benign non-aqueous solvents, but also tunable in structure and properties for a diverse range of reactions;[38,39] (ii) they can dissolve organic compounds ranging from low to high polarity, allowing organic reactants to enter droplets;[38] (iii) they are immiscible with some non-polar solvents, thus making it possible to generate IL-in-oil emulsion droplets through emulsification.[40,41] Here, particles are used as the emulsifier to stabilize emulsions (often termed Pickering emulsions) because particles at droplet interfaces have adsorption energies several orders of magnitude higher than conventional molecular surfactants,[42] leading to the high stability of the droplets against coalescence.[39-41,43,44] We found that dimethyldichlorosilane-modified silica nanospheres (40–60 nm) were an excellent emulsifier for diverse, commercially available, ILs ranging from hydrophobic ones like [BMIM]PF$_6$ (1-butyl-3-methylimidazolium hexafluorophosphate) and [BMIM]NTf$_2$ (1-butyl-3-methylimidazolium bis(trifluoromethylsulfonyl) imide) to hydrophilic ones like [BMIM]BF$_4$ (1-butyl-3-methylimidazolium tetrafluoroborate) and [BMIM]NO$_3$ (1-butyl-3-methylimidazolium nitrate), using a non-polar alkane or aromatic hydrocarbon as the continuous oil phase (Figure S1).[40,41] This particle emulsifier exhibits high hydrophobicity since the contact angle of a water drop in air was measured to be as high as 132° (Figure S2). The particles are non-porous and spherical in shape, with an average diameter of *ca.* 60 nm, as evidenced by N$_2$ sorption analysis and transmission electron microscopy (TEM) (Figure S3). Their surface composition was characterized by X-ray photoelectron spectroscopy (XPS) and elemental analysis (Figure S3).

Typically, by vigorously stirring a mixture of an IL and a non-polar oil for a few minutes, *e.g.* [BMIM]PF$_6$ and octane, in the presence of the particle emulsifier (the volume ratio of IL to oil is 2:1 and the emulsifier is 3 wt% with respect to the IL), we obtained an IL-in-octane Pickering emulsion, in which numerous IL droplets are present. Each droplet constitutes one micro-reactor with the IL enclosed in the interior and the emulsifier particles covering the surface of the droplets, confirmed by fluorescence dyeing experiments (Figures S4 and S5). These droplets are uniform in morphology of average diameter 36 μm (optical microscopy image in Figure 1B). Based on the average droplet diameter, it can be estimated that each droplet has a volume as small as *ca.* 2.4×10^{-11} L. Such nanoliter-scaled droplets are used as building blocks to construct a macroscale system through packing them in a column reactor (Figure 1A). Notably, there is a filter with micron-sized pores installed at the bottom of the column, preventing leakage of droplets from the column reactor, but allowing the continuous phase and the product dissolved in it, to pass through without difficulty. The size of the IL droplets can be readily tuned by varying the concentration of the silica particle emulsifier used. As shown in Figure S6, the average droplet diameter decreases from 103 to 23 μm upon increasing the concentration of particles from 1 to 5 wt %. This is simply explained by the fact that more particles need a larger interface area to occupy, leading to a decrease in the droplet size.[34,45] Interestingly, variation in the IL droplet size causes the change in the flow rate of the oil phase under the same applied pressure, with the larger droplets resulting in a higher flow rate of the oil phase, as shown in Figure 1C. The underlying reason is that at a fixed volume of IL, there is a larger number of droplets when they are small as compared to when they are large, and so the oil has to flow through finer channels between such droplets leading to a reduction of the flow rate.[34]

To examine the robustness of the IL droplets under conditions involving the flow of oil phase around them even at high temperature, the temperature of the column was raised to 80 °C and the flow rate of the oil phase was monitored. Over a period of 72 h, the flow rate of the oil remained constant (Figure 1D). Increasing the temperature to 90 °C and then further to 100 °C, the flow rate of the oil phase did not change over a further 144 h. The IL droplets remained intact without coalescing or aggregating, as evidenced from the optical micrographs (Figure S7). These observations prove that the particle-stabilized IL droplets are mechanically robust to withstand the continuous flow of the oil phase around them, even at these relatively high temperatures. The high stability originates from the high energy of desorption of the particles from the interface, which may be several orders of magnitude larger than the drag force caused by the liquid flow and the gravity to which the particles are also subjected.[34] Accordingly, the particle shell around the droplet interface provides a sturdy shield for the internal IL.

The IL droplets can serve as micro-containers to encapsulate catalysts such as an enzyme or a homogeneous catalyst.[38,46,47] In order to visualize their "encapsulation" efficiency towards catalysts and their ability to retain catalysts from flowing away with the oil phase, we labeled an enzyme (lipase CALB) with a fluorescence reagent (Rhodamine B).[48] The labeled enzyme can be easily encapsulated within the IL droplets through a one-step emulsification. This encapsulation procedure is rather straightforward as compared to the conventional methods for immobilization of enzymes, yet quite effective since all labeled enzyme is located inside the IL droplets and no fluorescence signals were found outside the droplets (Figure S8, A). The fluorescence intensity was found to be identical everywhere inside the droplet, indicating that the enzyme is homogeneously distributed inside the droplets (Figure 1E). Rather impressively, after 48 h

of continuous flow, the fluorescence intensity inside the IL droplets did not decay (Figure S8, B), whilst no fluorescence signals were observed in the effluent oil phase (Figure S8, C). These findings unambiguously verify that the IL droplets as micro-reactors have an excellent ability to confine CALB within them thus preventing its loss, even under conditions involving the flowing oil phase.

Next, we investigated the ability of the IL droplet to exchange molecular species with the outside oil phase, which is a pre-requisite for droplets acting as micro-reactors. Fluorescent probe reagents were used to visualize this process. The fluorescent reagent, Nile Red, initially present in the continuous oil phase, was observed to spontaneously enter the IL droplets, as demonstrated by the time-dependent fluorescence microscopy images of the IL droplets (Figure 2A) and the time-course fluorescence intensity (Figure 2B). Within a short duration of 0.5 min, fluorescence appears inside the IL droplets, indicating that the fluorescent molecules cross the IL-oil droplet interface and enter the droplets. In the subsequent times at 1.0, 1.5 and 2.0 min, the fluorescence intensity increases gradually as a result of an increase in the concentration of the fluorescent reagent inside the droplets, levelling off after 2.5 min. In parallel, another fluorescent reagent, FITC-I, was utilized to visualize molecular diffusion out of the
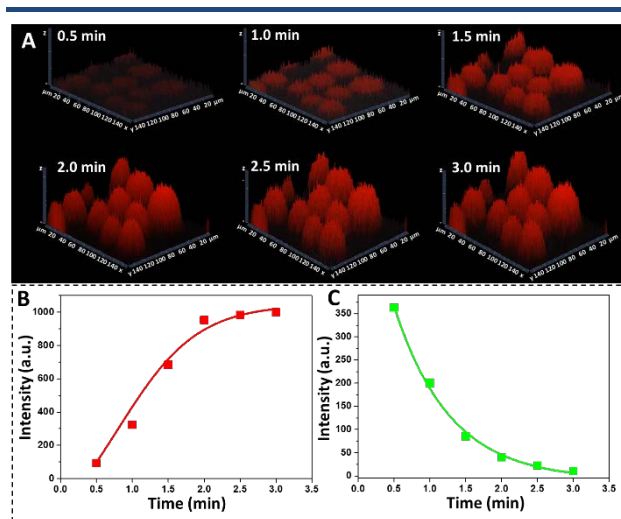

Figure 2. Fluorescence microscopy with time for the transport of probe molecules into/out of IL droplets in oil. (A) 3D confocal fluorescence microscopy images of the transport of Nile Red (5 μM) into the droplets. (B) Variation of fluorescence intensity with time for the transport of Nile Red into IL droplets. (C) Variation of fluorescence intensity with time for the transport of FITC-I (2 μM) out of IL droplets. The IL-in-octane Pickering emulsions consist of 2 g [BMIM]PF$_6$, 0.7 mL n-octane and 0.06 g solid emulsifier.

droplets. FITC-I initially present inside the IL droplets was observed to spontaneously diffuse very rapidly out of the droplets into the outer oil phase (Figure 2C and Figure S9). These experiments suggest that the particle shell around the surface of the IL droplet has no substantial effect on the transport of reactants and products across the IL-oil interface. These results also confirm that molecular transport both into and out of the IL droplets proceeds very quickly, since the observed timescales are as small as a few minutes. Such a rapid molecular communication with the outside oil phase is quite beneficial to catalysis reactions occurring inside the IL droplets.[36]

2.2. Continuous Flow Catalysis Reaction. Having demonstrated the stability of IL droplets, and their ability to confine catalysts and exchange molecular species with the outer oil phase, we next investigate their utility in processing enzymatic and homogeneous catalysis reactions.

Enzymatic enantioselective trans-esterification of alcohols,[2,13,49] in which one of the alcohol enantiomers is selectively converted to a chiral ester while leaving the other enantiomer unreacted, was chosen as a model reaction. This reaction is of practical importance in obtaining chiral alcohols and chiral esters, but often surfers from the product inhibition effect.[2,13] Similar to the above procedure, an IL-in-oil Pickering emulsion was formulated in the presence of a lipase CALB. This emulsion was then poured into a column reactor, yielding an IL droplet-packed bed for catalysis. A solution of racemic 4-phenyl-2-butanol and vinyl acetate (acylating agent) in octane was continuously pumped into the inlet of this factory and the product-containing stream was collected from the outlet of the factory and analyzed with GC at different times. To screen out a good IL for this reaction, we first examined the specific activity of CALB in different ILs, including [BMIM]PF$_6$, [BMIM]NTf$_2$, [BMIM]BF$_4$, and [BMIM]NO$_3$. Of these, [BMIM]PF$_6$ gave the highest specific activity under identical conditions (Figure S10), which is consistent with the previously reported results of the reaction in bulk ILs.[46] The resultant enantiomeric excesses (ee values) of alcohol and ester are plotted as a function of time in Figure 3A. The ee value of the alcohol rapidly rose up to 99%, and the ee value of the ester was always 99% once it came out of the column. These values were maintained at 99% with only slight fluctuations for alcohol over a period of 720 h, although the flow rate was required to be tuned from an initial 2.5 mL h^{-1} to 2 mL h^{-1} at the end of the experiment. For other substrates such as 1-indanol and 4-methyl-2-pentanol, ee values of 90–99% for alcohols and esters were also maintained over a course of 720 h (Figure 3B and Figure 3C). For the less reactive substrates such as 5-methyl-3-hexanol and 1-phenylethylamine, the corresponding ester and amide with 99% ee values were
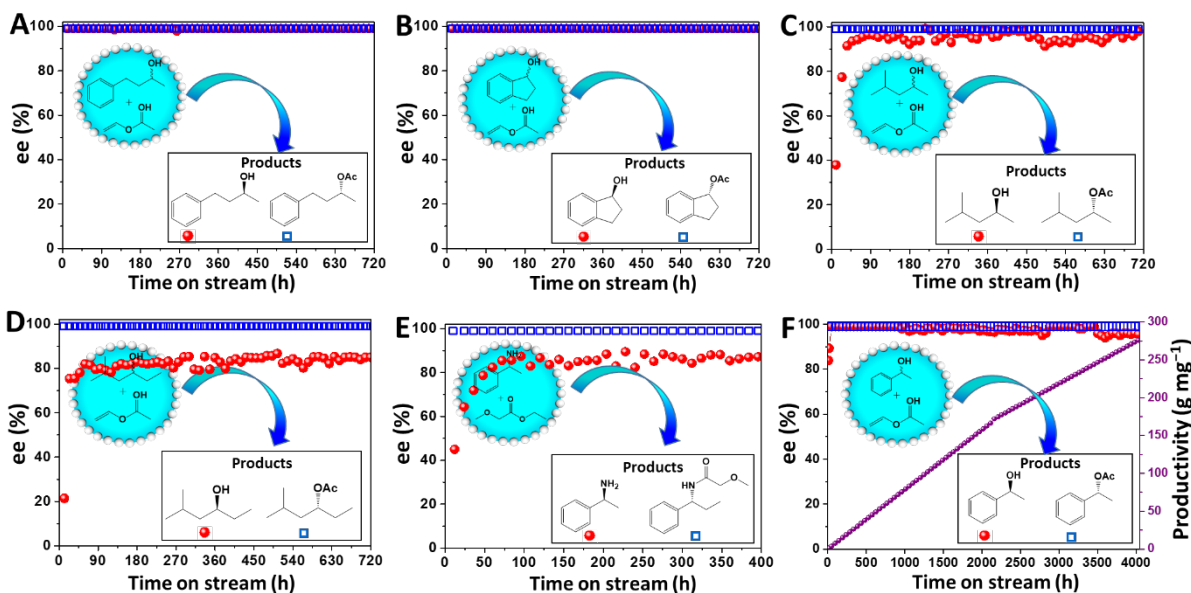
Figure 3. CALB-catalyzed enantioselective trans-esterification and amidation in the IL-based continuous flow systems. The column diameter used in reactions is 2.0 cm, red points are alcohol or amine product, blue points are ester or amide product and purple points are productivity. The IL-based Pickering emulsions consist of 80 μL (for alcohols) or 240 μL (for amine) aqueous enzyme solution (4 mg mL^{-1} of protein; pH 8.0) dispersed in 6.5 g [BMIM]PF$_6$, 2.4 mL n-octane or toluene and 0.195 g emulsifier. Reaction conditions: mobile phase is a solution of racemic alcohol (0.1 M) or racemic amine (0.05 M) and vinyl acetate (for alcohols, 0.4 M) or ethyl methoxyacetate (for amine, 0.2 M) in n-octane or toluene, 45 °C. (A) 4-Phenyl-2-butanol, n-octane, flow rate from initial 2.5 mL h^{-1} to 2 mL h^{-1} at the end; (B) 1-Indanol, n-octane, flow rate from initial 2.5 mL h^{-1} to 2 mL h^{-1} at the end; (C) 4-Methyl-2-pentanol, n-octane, flow rate from initial 0.6 mL h^{-1} to 0.4 mL h^{-1} at the end; (D) 5-Methyl-3-hexanol, n-octane, flow rate from initial 0.25 mL h^{-1} to 0.2 mL h^{-1} at the end; (E)1-Phenylethylamine, toluene, flow rate from initial 0.6 mL h^{-1} to 0.5 mL h^{-1} at the end; (F) 1-Phenylethyl alcohol, n-octane, flow rate from initial 2 mL h^{-1} to 1.5 mL h^{-1} at the end.

still obtained over the same period of 720 h, although the corresponding ee values for alcohol and amine were 83% and 86%, respectively (Figure 3D and Figure 3E). After such a long period of continuous reaction, the droplet micro-reactors in all of the IL-based flow systems were still well preserved in terms of both their size and morphology (Figure S11). These results confirm that the IL droplet-based chemical factory is indeed viable to process enzymatic reactions in a continuous flow manner.

The long-term stability of the reaction system is of utmost importance if it is to be realistically utilized in practical applications. To test this, we prolonged the running time to a period as long as 4000 h. For the enantioselective trans-esterification of 1-phenylethyl alcohol to 1-phenylethyl acetate, the ee values of the generated alcohol and ester were still maintained at 95–99% with only slight fluctuations for alcohol, albeit at the expense of the flow rate decreasing from 2.0 mL h^{-1} at the start to 1.5 mL h^{-1} at the end (Figure 3F). No leakage of IL was observed after such a long period of time. The morphology and size of the IL droplets are essentially unchanged (Figure S11, F). The productivity

of the enzyme, estimated on the basis of g of product per mg enzyme, increases linearly with time (Figure 3F). After 4000 h, 44 g of enantiopure alcohol and 59 g of enantiopure 1-phenylethyl acetate were obtained after removal of octane from the collected effluent. The productivity of enzyme is as high as 272 g mg^{-1}, meaning that 1 g of enzyme can deal with 272 kg of 1-phenylethyl alcohol. As far as we know, these findings represent an unprecedented result, which far exceeds the industrially desirable standards (10-100 g product/g biocatalyst).[50] After 4000 h of continuous reaction, the specific activity of CALB was determined at relatively low conversions at a higher flow rate (3 mL h^{-1}). It was found that 77% of the initial specific activity of CALB was still maintained (Figure S12). The outstanding ability to retain this activity is attributed to two factors: (i) good capability of the IL droplet micro-reactors to prevent the enzyme from flowing away with the oil phase, which is supported by the aforementioned fluorescence observation (Figure S8); (ii) avoiding the direct contact of the enzyme with the oil phase which often causes deactivation of enzymes.[46]
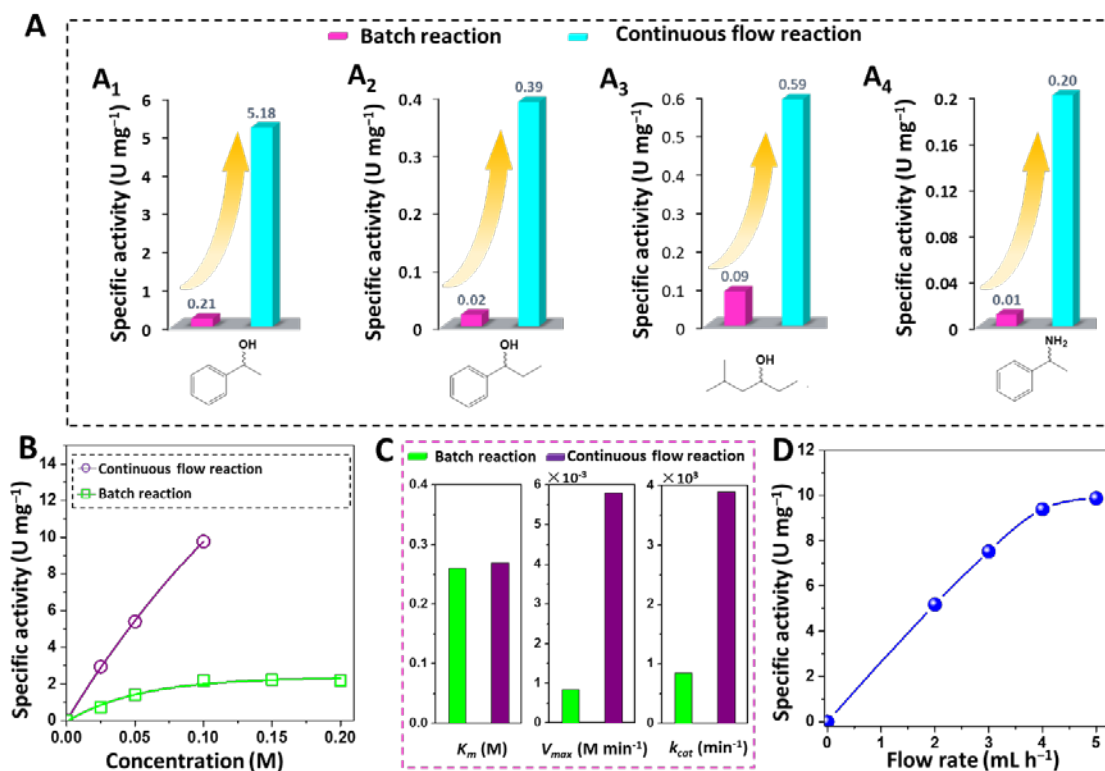
Figure 4. Comparison of CALB-catalyzed enantioselective trans-esterification and amidation in the biphasic batch reactions and in the IL droplet-based flow reactions. Specific activity (U mg^{-1}) is expressed as μmol of substrate converted per min per mg enzyme (*i.e.* μmol min^{-1} mg^{-1}). Batch reaction conditions: 2 g of [BMIM]PF$_6$ containing 25 μL (for alcohols) or 75 μL (for amine) aqueous enzyme solution (4 mg mL^{-1} of protein; pH 8.0), 1 mL of *n*-octane or toluene containing racemic alcohols (0.1 M) or racemic amine (0.05 M) and vinyl acetate (for alcohols, 0.4 M) or ethyl methoxyacetate (for amine, 0.2 M), 45 °C, 2600 rpm. The IL droplet-based continuous flow reactions conditions are the same as in Figure 3 except the concentration of substrates or the flow rate of the oil phase. (A) Specific activity of CALB in the batch reaction calculated over 720 min and that in the IL droplet-based flow reactions calculated at steady state. (A$_1$) 0.1 M 1-phenylethyl alcohol in *n*-octane, 2 mL h^{-1} flow rate for the flow system, (A$_2$) 0.1 M 1-phenyl-1-propanol in *n*-octane, 0.25 mL h^{-1} flow rate, (A$_3$) 0.1 M 5-methyl-3-hexanol in *n*-octane, 0.25 mL h^{-1} flow rate, (A$_4$) 0.05 M 1-phenylethylamine in toluene, 0.5 mL h^{-1} flow rate. (B) Initial specific activity of CALB at different concentrations of 1-phenylethyl alcohol in the batch reactions within first 20 min, and specific activity of CALB in the droplet-based continuous flow at different concentrations of 1-phenylethyl alcohol at steady state (5 mL h^{-1}); (C) Comparison of K_m, V_{max} and k_{cat} between the batch reaction and IL droplet-based flow reactions; (D) Specific activity of CALB in the flow system as a function of the flow rate.

We further evaluated the specific activity of CALB in the continuous flow system by comparison with conventional batch reactions (Figure 4A and Figure S13). Due to the high viscosity of the IL, the batch reaction was conducted under high speed stirring conditions (2600 rpm). For 1-phenylethyl alcohol as a substrate, the batch reaction gave an ee value of 16.5% for 1-phenylethyl alcohol after 12 h (Figure S13, A). Further prolonging of the reaction time did not result in any increase in the ee value. A leveling off of the ee value with time means that the trans-esterification reaction suffered from a strong product inhibition effect. Based on the ee values obtained, we estimate the specific activity of the enzyme in the batch reaction to be 0.21 U mg^{-1}. In contrast, the flow system provides 1-phenylethyl alcohol with an ee 99% such that the specific activity is

as high as 5.18 U mg^{-1}, which is a 25-fold enhancement when compared with the batch reaction (Figure 4A1), and 2.4 times higher than the initial specific activity in the batch reaction (Figure S13). Such a striking contrast is also found for 1-phenyl-1-propanol, 5-methyl-3-hexanol and 1-phenylethylamine as substrates. As displayed in Figure 4A2, for 1-phenyl-1-propanol, the specific activity of CALB in the flow system is 0.39 U mg^{-1}, *i.e.* 20-fold higher than that achieved in the batch reaction. For 5-methyl-3-hexanol, the specific activity of CALB in the flow system was 0.59 U mg^{-1}, which is 7 times higher than that in the corresponding batch reaction (Figure 4A3). For the amidation of 1-phenylethylamine, the specific activity of CALB in the flow system is 0.20 U mg^{-1}, which is 20-fold higher than that obtained in the batch reaction (Figure 4A4). The

results from all these cases point to a general trend indicating that the flow system can substantially boost the catalysis efficiency of enzymatic reactions,[12,13] delivering the superiority of continuous flow reactions over batch reactions.[51-56]

In order to further evaluate the impact of the flow of the continuous phase on the performance of enzyme, we determined the kinetic parameters of CALB in the continuous flow system and in the batch system by changing the concentration of reactants (Figure 4B and Figure S14), yielding the apparent Michaelis-Menten constant K_m, the maximal reaction rate V_{max} (rate of the reaction when the active sites of the enzyme are saturated with substrate) and the turnover number k_{cat} (Figure 4C and Figure S15).[57] As displayed in Figure 4C, K_m for the flow system is calculated as 0.27 M, which was found to be equal to that for the batch reaction. This finding suggests a similar affinity between the substrate and enzyme for these two reaction systems due to the similar reaction micro-environment. However, as shown in Figure 4B, the specific activity of CALB in these two systems shows a significantly different concentration-dependent effect. These data allow us to estimate V_{max} in the flow system to be 5.8×10^{-3} M min^{-1}, which is 7-fold higher than that in the batch system. Moreover, k_{cat} in the flow system was 5-times higher than that in the batch reaction. The significant increase in the kinetic parameters V_m and k_{cat} further confirms that the CALB in the droplet-based flow system has high catalysis efficiency. The underlying

reason we believe, relates to the fact that the IL droplet-based flow system manages to drastically decrease the product inhibition due to the timely and efficient removal of product from the reaction system,.[12,13] As a result, the continuous flow maintains the reaction away from equilibrium and is biased in favor of product formation.[35,36] The comparative experiments, including the reaction in the column reactor without flow (Figure S16), the introduction of the product at the beginning of reaction (Figure S17) and the enzymatic reaction without severe product inhibition effects (Figure S18), all verify this finding. Our inference is further supported by the findings that the higher flow rate of the oil phase led to the larger specific activity (Figure 4D and Figure S19). Taken together, all of the above results corroborate the fact that the IL droplet-based flow catalysis system is a truly competitive means for the practical application of enzymes in view of its high efficiency, decreased product inhibition effect, excellent duration and cost-effectiveness.

To explore the generality of the method, we apply this IL-based flow strategy to a chemocatalysis reaction, for example CuI-catalyzed azide–alkyne cycloaddition.[58,59] This reaction is an important route to access 1,4-di-substituted 1,2,3-triazoles (Figure 5A). In the batch system, it took 11 h to obtain 98.5% conversion of benzyl azide (Figure 5B). Its catalysis efficiency was calculated to be 0.053 mol mol^{-1} h^{-1} (Figure 5D). When utilizing the flow reaction instead of the batch one, the conversion of phenyl acetylene at steady state was more than 99.9%
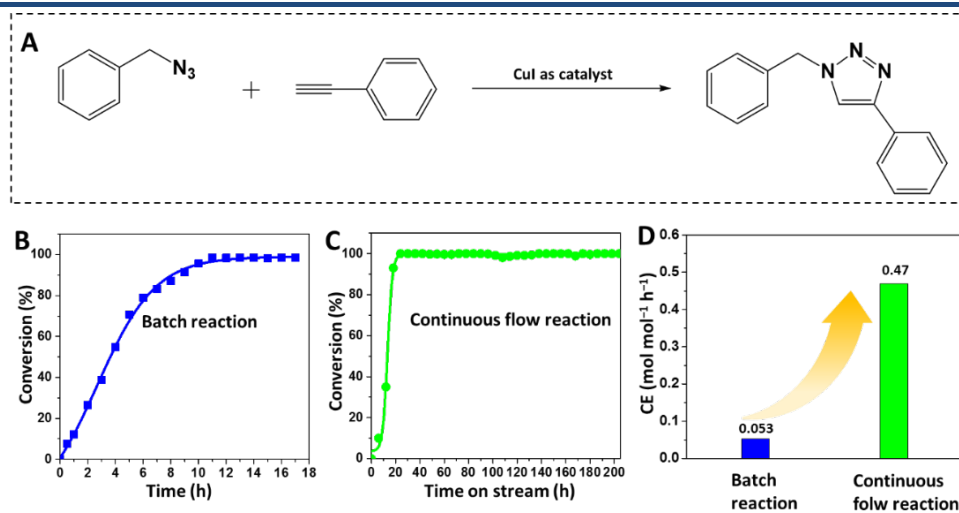

Figure 5. CuI-catalyzed azide–alkyne cycloadditions in the batch system and in the IL droplet-based flow system. (A) Cycloaddition reaction, (B) Kinetic profile for the cycloaddition of benzyl azide and phenyl acetylene in the batch system, (C) Conversion with time for the cycloaddition of benzyl azide and phenyl acetylene in the IL droplet-based flow system, (D) Catalysis efficiency (CE) of CuI in the batch system and in the IL droplet-based flow system. For the batch system, CE is calculated according to the conversion within the first 11 h. For the flow system, CE is calculated after the conversion levelled off at steady state. Batch reaction conditions: 2 g [BMIM]PF$_6$, 0.032 g CuI, 0.16 g L-ascorbic acid sodium (as antioxidant dispersed in IL), 1 mL solution of benzyl azide (0.1 M) and phenyl acetylene (0.12 M) in a mixture of *n*-octane and toluene (v/v = 1:1), 25 °C, 2600 rpm. Continuous flow reaction conditions: IL-in-oil Pickering emulsion consists of 2 g [BMIM]PF$_6$, 0.032 g CuI, 0.16 g L-ascorbic acid sodium, 0.7 mL of a mixture of *n*-octane and toluene (v/v = 1:1), 0.06 g emulsifier, a solution of benzyl azide (0.1 M) and alkyne (0.12 M) in a mixture of *n*-octane and toluene (v/v = 1:1) as mobile phase, 25 °C, flow rate from initial 0.8 mL h^{-1} to 0.5 mL h^{-1} at the end.

(Figure 5C) and the catalysis efficiency was 0.47 mol mol⁻¹ h⁻¹ (Figure 5D), which is 9-fold higher than that obtained in the batch reaction. Moreover, over a duration of 200 h on stream, the conversion showed no apparent decrease, although the flow rate had to be decreased slightly. The 73% CuI used initially in the flow reaction was retained in the IL droplets as found by inductively coupled plasma mass spectrometry (ICP-MS), highlighting the high stability of our flow system. Another substrate, 1-hexyne, was also efficiently converted in the IL-based flow system exhibiting 4.4-fold enhanced efficiency and long term stability (Figure S20). These results yet again demonstrate the high flexibility of the "chemical factory" in processing chemocatalysis reactions, as well as further underlining the generic point that our IL-based flow system can also significantly boost the catalysis efficiency of chemocatalysis reactions and enzymatic reactions.

2.3. Theoretical Investigation. In order to further understand the reasons for the enhanced catalysis efficiency in the IL droplet-based flow system for either enzymatic reactions or chemocatalysis reactions, we establish the key principles underlying the continuous flow system. On the length scale of a single droplet, it is appropriate to assume spherical symmetry around each droplet, as any differences between the environment at the top and bottom of a single droplet arising from the flow of the continuous phase are negligible (section 9 of Supporting Information). We first start by writing down the kinetic equations inside a droplet micro-reactor that theoretically describe the localized reactions occurring inside the droplets. A general reaction, A+B⇌C, is considered here. The reactants A and B diffuse into the droplet and in turn the product C, generated by the reaction inside the droplet, diffuses out. Under steady state conditions, the following equations describe the mass balance inside the droplet:

$$\frac{D_{IL}^A}{r^2}\frac{\partial}{\partial r}\left(r^2\frac{\partial[A]}{\partial r}\right) - k_1[A][B] + k_2[C] = 0 \quad (1)$$

$$\frac{D_{IL}^B}{r^2}\frac{\partial}{\partial r}\left(r^2\frac{\partial[B]}{\partial r}\right) - k_1[A][B] + k_2[C] = 0 \quad (2)$$

$$\frac{D_{IL}^C}{r^2}\frac{\partial}{\partial r}\left(r^2\frac{\partial[C]}{\partial r}\right) + k_1[A][B] - k_2[C] = 0 \quad (3)$$

where [A] and [B] denote the concentrations of reactants A and B, and [C] represents the concentration of the product. The parameters D_{IL}^A, D_{IL}^B and D_{IL}^C are the diffusion coefficients of A, B and C in the dispersed IL phase. Similarly, k_1 and k_2 are the rate constants of the forward and backward reactions, occurring inside the droplets. The radial distance from the center of the droplet is denoted by r.

To simplify the calculations, we may take the concentration of one of the reactants which is in excess (for example B) to be more or less constant (denoted by B_{IL}^0), within the droplet and similarly outside it. Therefore, we only need to focus on equations (1) and (3)

above. By solving these equations (section 9 of Supporting Information), we obtain the concentration profiles of A and C along r, which are found to be

$$A(r) = \frac{q}{D_{IL}^A}\left(1 - \frac{K[B]_{IL}^0 D_{IL}^C}{K[B]_{IL}^0 D_{IL}^C + D_{IL}^A}\right) - \frac{2nD_{IL}^C \sinh(r/\zeta)}{rD_{IL}^A} \quad (4)$$

$$C(r) = \lambda\zeta^2 + \frac{2n}{r}\sinh(r/\zeta) \quad (5)$$

where q and n are the integration constants which can be calculated through consideration of boundary conditions at the interface of the droplet, at its center and far away from it. Also in the above equations the constant K is the equilibrium constant for the reaction, (k_1/k_2), while λ and ζ are defined as $\lambda = (k_1 B_{IL}^0 q)/(D_{IL}^C D_{IL}^A)$ and $\zeta^{-2} = (k_1 B_{IL}^0 / D_{IL}^A) + (k_2 / D_{IL}^C)$.

In contrast to the reaction inside the IL droplet, the reaction in the oil does not occur due to the absence of any catalysts in this phase. Accordingly, the reaction-diffusion equations reduce to simple diffusion ones, *i.e.*

$$\frac{D_{Oil}^A}{r^2}\frac{\partial}{\partial r}\left(r^2\frac{\partial[A]}{\partial r}\right) = 0 \quad (6)$$

$$\frac{D_{Oil}^C}{r^2}\frac{\partial}{\partial r}\left(r^2\frac{\partial[C]}{\partial r}\right) = 0 \quad (7)$$

By solving these two equations (section 9 of Supporting Information) we can obtain the concentration profiles of A and C in the radial direction away from the droplet in the oil phase:

$$A(r) = [A]_{Oil}^0 - \frac{1}{r}\left(\begin{array}{c} R[A]_{Oil}^0 - \frac{qR}{\alpha_A D_{IL}^A}\left(1 - \frac{K[B]_{IL}^0 D_{IL}^C}{K[B]_{IL}^0 D_{IL}^C + D_{IL}^A}\right) \\ + \frac{2nD_{IL}^C \sinh(R/\zeta)}{\alpha_A D_{IL}^A} \end{array}\right) \quad (8)$$

$$C(r) = [C]_{Oil}^0 - \frac{1}{r}\left(R[C]_{Oil}^0 - \frac{R\lambda\zeta^2}{\alpha_C} - \frac{2n}{\alpha_C}\sinh(R/\zeta)\right) \quad (9)$$

The boundary conditions can be established when the reactions reach the steady state. The fluxes of A and C entering and leaving the droplet interface, between the IL and oil, have to be equal under such circumstances (assuming no additional specific reactions taking place on the interface). This is expressed as follows:

$$D_{IL}^A \frac{\partial[A]}{\partial r}\bigg|_{R^-} = D_{Oil}^A \frac{\partial[A]}{\partial r}\bigg|_{R^+} \quad (10)$$

$$D_{IL}^C \frac{\partial[C]}{\partial r}\bigg|_{R^-} = D_{Oil}^C \frac{\partial[C]}{\partial r}\bigg|_{R^+} \quad (11)$$

where R⁻ refer to the points infinitely close to the internal droplet surface within the IL, and R⁺ refer to the points infinitely close to the external droplet surface in the oil phase We denote the diffusion coefficients of A and C in the continuous oil phase as D_{Oil}^A and D_{Oil}^C. The concentrations of A and C immediately close to either side of the interface are at equilibrium with each other, as dictated by the partition coefficient between IL and oil for each of these components.

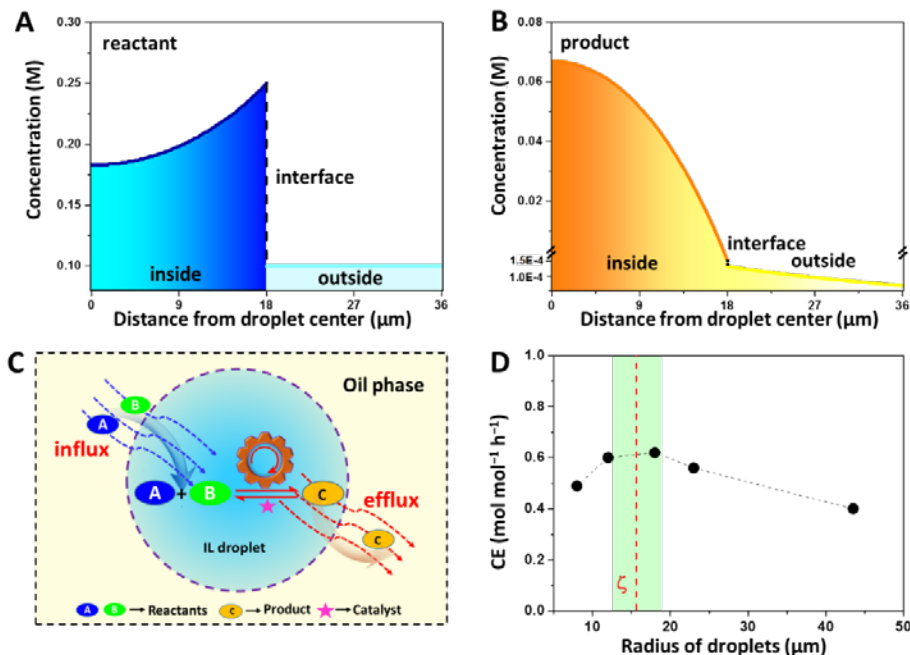Substituting equations (4), (5), (8) and (9) into the

Figure 6. Theoretical investigation into the driving force for the reaction occurring inside a single droplet. (A) Calculated concentration profile of benzyl azide reactant from the centre of the IL droplet to the oil phase. (B) Calculated concentration profile of 1-benzyl-4-phenyl-1,2,3-triazole product from the centre of the IL droplet to the oil phase. (C) Schematic illustration of a general reaction (A+B⇌C) within the IL droplet. (D) Catalysis efficiency of the cycloaddition reaction *versus* droplet radius. The IL-in-ol Pickering emulsion consists of 2 g [BMIM]PF$_6$, 0.032 g CuI, 0.16 g L-ascorbic acid sodium (as antioxidant), 0.7 mL of a mixture of *n*-octane and toluene (v/v = 1:1) with the amount of solid emulsifier ranging from 1 wt % to 2 wt % to 3 wt % to 4 wt % and 5 wt % (with respect to IL). Mobile phase was a solution of benzyl azide (0.1 M) and phenyl acetylene (0.12 M) in a mixture of *n*-octane and toluene (v/v = 1:1), 25 °C, flow rate = 1.5 mL h^{-1}.

boundary equations (10) and (11), and making use of the equilibrium condition on both sides of the interface, we arrive at the following results for the integration constants q and n,

$$q = \frac{w_2 u_1 - w_1 u_2}{w_2 v_1 - w_1 v_2} \tag{12}$$

$$n = \frac{u_1}{w_1} - \frac{v_1}{w_1}\left(\frac{w_2 u_1 - w_1 u_2}{w_2 v_1 - w_1 v_2}\right) \tag{13}$$

where, $u_1 = R[A]_{Oil}^0\left(\dfrac{D_{IL}^A}{D_{IL}^C}\right)$, $v_1 = \dfrac{R}{\alpha_A D_{IL}^C}\left(1 - \dfrac{k_1[B]_{IL}^0 \zeta^2}{D_{IL}^A}\right)$,

$w_1 = 2\left[\dfrac{D_{IL}^A}{D_{Oil}^A}\sinh(R/\zeta) - \dfrac{1}{\alpha_A}\sinh(R/\zeta) - \dfrac{RD_{IL}^A}{\zeta D_{Oil}^A}\cosh(R/\zeta)\right]$,

$u_2 = -R[C]_{Oil}^0$, $v_2 = -\dfrac{R}{\alpha_C D_{IL}^A}\left(\dfrac{k_1[B]_{IL}^0 \zeta^2}{D_{IL}^C}\right)$,

$w_2 = 2\left[\dfrac{D_{IL}^C}{D_{Oil}^C}\sinh(R/\zeta) - \dfrac{1}{\alpha_C}\sinh(R/\zeta) - \dfrac{RD_{IL}^C}{\zeta D_{Oil}^C}\cosh(R/\zeta)\right]$

The partition coefficients of A and C between the IL and the oil phase ([reagent]$_{IL}$/[reagent]$_{oil}$) are represented by α_A and α_C, respectively, in the above set of equations. Taking these into account and using equations (4) and (5), the concentration profiles of reactant A and product C along the droplet radius can finally be evaluated in terms of measurable parameters, *i.e.* diffusion coefficients, radius of droplet, R, partition coefficients, reaction rate constants and finally the concentration of A and C within the oil phase far from the droplet, $[A]_{Oil}^0$ and $[C]_{Oil}^0$

$$A(r) = \frac{1}{D_{IL}^A}\left(\frac{w_2 u_1 - w_1 u_2}{w_2 v_1 - w_1 v_2}\right)\left(1 - \frac{K[B]_{IL}^0 D_{IL}^C}{K[B]_{IL}^0 D_{IL}^C + D_{IL}^A}\right)$$
$$- \frac{2D_{IL}^C}{rD_{IL}^A}\left(\frac{u_1}{w_1} - \frac{v_1}{w_1}\left(\frac{w_2 u_1 - w_1 u_2}{w_2 v_1 - w_1 v_2}\right)\right)\sinh(r/\zeta) \tag{14}$$

$$C(r) = \lambda\zeta^2 + \frac{2}{r}\left(\frac{u_1}{w_1} - \frac{v_1}{w_1}\left(\frac{w_2 u_1 - w_1 u_2}{w_2 v_1 - w_1 v_2}\right)\right)\sinh(r/\zeta) \tag{15}$$

For a given reaction, for example, the above cycloaddition reaction, substituting the appropriate parameters into equations (14) and (15) the concentration profiles for the reactant and product inside the droplet as a function of the radial distance away from the center of the droplet can now be plotted. As shown in Figure 6A, the concentration of reactant is

maximum at the droplet interface and gradually decreases towards the droplet center. Conversely, the concentration of the product gradually decreases from the droplet center to the interface (Figure 6B). In spite of the difficulty in practical determination of the concentration profiles, these calculated results seem quite sensible. As we move along the radial direction, from the interface to the center, an increasing amount of reactant is converted into product. This calculation reveals that there exists a concentration gradient along the radius for both reactant and product, depending on any given set of parameters.

These derived profiles are helpful in understanding the driving force for the reaction inside the droplets. Molecular diffusion arising from a concentration gradient can cause molecules to migrate spontaneously from regions of high concentration to ones of low concentration. Due to the constant supply of reactants and simultaneous removal of the products, such concentration gradients for both reactants and products are always maintained during the stream time. Such a "never-ending" diffusion of the reactants into the droplets and the constant removal of the products from droplets ensure that the reaction inside each micro-reactor is maintained away from the equilibrium state in a manner that favors the forward reaction (Figure 6C). Consequently, catalysis efficiency is greatly enhanced.[35,36] Numerous such micro-reactors work efficiently together in parallel, resulting in significantly improved reaction efficiency on a macroscopic scale in comparison to the conventional batch reactions. In the latter, once equilibrium is reached the net reaction no longer progresses further.

Moreover, the theoretical profiles provide a framework to predict spatially the reaction occurring inside the droplet, and to guide the selection of parameters such as droplet size, partition coefficient, reaction rate constant, equilibrium constant and diffusion coefficient. As an example, it is very interesting to note from equations (14) and (15), the reaction occurs mainly within a shell of thickness ζ just inside the droplets away from the interface. This sets an upper limit on the size of the droplets, above which a certain part of the IL phase (*i.e.* IL not inside this shell of thickness ζ) is no longer usefully utilized. Consequently the optimum droplet size is expected to be $R \sim \zeta$. When $R > \zeta$ reactant molecules would be consumed completely before arriving at the center of the droplet. In contrast, when $R < \zeta$ the smaller droplets would lead to a lower catalysis efficiency, since some substrate molecules do not have sufficient time to react before diffusing out of the droplets. This inference is supported by experiments in which the IL droplet size is varied in the CuI-catalyzed cycloaddition of benzyl azide and phenyl acetylene (Figure 6D, Figures S21, S22 and S23). These results highlight the importance of the size of the IL

droplet micro-reactor. Obviously, such a precise regulation of IL droplet micro-reactors enables one a great degree of control over the macroscale flow reaction, in a "bottom-up" type method.

3. CONCLUSION

We have successfully developed a novel catalysis system based on the use of particle-stabilized IL droplets in oil as micro-reactors to construct a continuous flow catalysis system in a "bottom-up" fashion. Such a flow system was proven to be very powerful for the continuous use of enzymes and homogeneous catalysts boosting catalysis efficiency. Impressively, after 4000 h on stream for the enantioselective trans-esterification of 1-phenylethyl alcohol, the catalysis efficiency shows no significant decrease, highlighting an excellent durability and an outstanding level of productivity. Interestingly, the catalysis efficiency in the flow system is improved eight to twenty five-fold in comparison to their batch homogeneous counterparts. The continuous supply of substrates to droplet micro-reactors and rapid removal of products from them makes the compartmentalized reactions remain in a non-equilibrium state even when steady state is achieved. As a result, the reactions inside the droplets are always biased towards the forward direction. A huge number of such micro-reactors all working together in parallel result in a significantly boosted catalysis efficiency of the reaction, when viewed on macroscale. Furthermore, the theoretical model for this system was established here, not only supporting the experimental results but also allowing us to predict the reaction progressing inside the IL droplet micro-reactor in terms of measurable parameters. Being operationally simple and at the same time efficient and adaptive, our IL droplet-based flow system provides an unprecedented platform for practical applications of enzymes and homogeneous catalysts even at a controllable level.

ASSOCIATED CONTENT

Supporting Information
Experimental details; TEM images; Water contact angles; Appearance of Pickering emulsions; Optical microscopy image; Theoretical investigation; Equation derivation process; Reaction kinetics monitoring and MS data for products. This material is available free of charge via the Internet at http://pubs.acs.org.

AUTHOR INFORMATION

Corresponding Author

*hqyang@sxu.edu.cn

Notes
The authors declare no competing financial interests.

ACKNOWLEDGMENT

REFERENCES

(1) Cole-Hamilton, D. J. *Science* **2003**, *299*, 1702.

(2) Koeller, K. M.; Wong, C. H. *Nature* **2001**, *409*, 232.

(3) DiCosimo, R.; McAuliffe, J.; Poulose, A. J.; Bohlmann, G. *Chem. Soc. Rev.* **2013**, *42*, 6437.

(4) Tzschucke, C. C.; Markert, C.; Bannwarth, W.; Roller, S.; Hebel, A.; Haag, R. *Angew. Chem., Int. Ed.* **2002**, *41*, 3964.

(5) Yang, Y.; Zhang, B.; Wang, Y. Z. Yue, L.; Li, W.; Wu, L. X. *J. Am. Chem. Soc.* **2013**, *135*, 14500.

(6) Koszelewski, D.; Lavandera, I.; Clay, D.; Guebitz, G. M.; Rozzell, D.; Kroutil, W. *Angew. Chem., Int. Ed.* **2008**, *47*, 9337.

(7) Valera, F. E.; Quaranta, M.; Moran, A.; Blacker, J.; Armstrong, A.; Cabral, J. T.; Blackmond, D. G. *Angew. Chem., Int. Ed.* **2010**, *49*, 2478.

(8) Stitt, E. H. *Chem. Eng. J.* **2002**, *90*, 47.

(9) Webb, P. B.; Sellin, M. F.; Kunene, T. E.; Williamson, S.; Slawin, A. M. Z.; Cole-Hamilton, D. J. *J. Am. Chem. Soc.* **2003**, *125*, 15577.

(10) Kopach, M. E.; Roberts, D. J.; Johnson, M. D.; Groh, J. M.; Adler, J. J.; Schafer, J. P.; Kobierski, M. E.; Trankle, W. G. *Green Chem.* **2012**, *14*, 1524.

(11) Chen, Z. W.; Zhou, L.; Bing, W.; Zhang, Z. J.; Li, Z. H.; Ren, J. S.; Qu, X. G. *J. Am. Chem. Soc.* **2014**, *136*, 7498.

(12) Denčić, I.; de Vann, S.; Noël, T.; Meuldijk, J.; de Croon, M.; Hessel, V. *Ind. Eng. Chem. Res.* **2013**, *52*, 10951.

(13) Sandig, B.; Buchmeiser, M. R. *ChemSusChem* **2016**, *9*, 2917.

(14) Özdural, A. R.; Tanyolaç, D.; Boyacı, İ. H.; Mutlu, M.; Webb, C. *Biochem. Eng. J.* **2013**, *14*, 27.

(15) Zhang, W. J.; Fu, L. M.; Yang, H. Q. *ChemSusChem* **2014**, *7*, 391.

(16) Cents, A. H. G.; Brilman, D. W. F.; Versteeg, G. F. *Ind. Eng. Chem. Res.* **2004**, *43*, 7465.

(17) Qiao, Y. X.; Ma, W. B.; Theyssen, N.; Chen, C.; Hou, Z. S. *Chem. Rev.* **2017**, *117*, 6881.

(18) Geldbach, T. J.; Zhao, D. B.; Castillo, N. C.; Laurenczy, G.; Weyershausen, B.; Dyson, P. J. *J. Am. Chem. Soc.* **2006**, *128*, 9773.

(19) Sievers, C.; Noda, Y.; Qi, L.; Albuquerque, E. M.; Rioux, R. M.; Socct, S. L. *ACS Catal.* **2016**, *6*, 8286.

(20) Shang, L. R.; Chen, Y.; Zhao, Y. J. *Chem. Rev.* **2017**, *117*, 7964.

(21) Elvira, K. S.; Solvas, X. C. i.; Wootton, R. C. R.; deMello, A. J. *Nat. Chem.* **2013**, *5*, 905.

(22) Riche, C. T.; Roberts, E. J.; Gupta, M.; Brutchey, R. L.; Malmstadt, N. *Nat. Commun.* **2016**, *7*, 10780.

(23) Deng, N. N.; Yelleswarapu, M.; Zheng, L. F.; Huck, W. T. S. *J. Am. Chem. Soc.* **2016**, *138*, 7584.

(24) Song, H.; Chen, D. L.; Ismagilov, R. F. *Angew. Chem., Int. Ed.* **2006**, *45*, 7336.

(25) Theberge, A. B.; Courtois, F.; Schaerli, Y.; Fischlechner, M.; Abell, C.; Hollfelder, F.; Huck, W. T. S. *Angew. Chem., Int. Ed.* **2010**, *49*, 5846.

(26) Yan, X.; Bain, R. M.; Cooks, R. G. *Angew. Chem., Int. Ed.* **2016**, *55*, 12960.

(27) Chen, P. C.; Du, J. S.; Meckes, B.; Huang, L. L.; Xie, Z.; Hedrick, J. L.; Dravid, V. P.; Mirkin, C. A. *J. Am. Chem. Soc.* **2017**, *139*, 9876.

(28) Crossley, S.; Faria, J.; Shen, M.; Resasco, D. E. *Science* **2010**, *327*, 68.

(29) Piradashvili, K.; Alexandrino, E. M.; Wurm, F. R.; Landfester, K. *Chem. Rev.* **2016**, *116*, 2141.

(30) Pera-Titus, M.; Leclercq, L.; Clacens, J. M.; De Campo, F.; Nardello-Rataj, V. *Angew. Chem., Int. Ed.* **2015**, *54*, 2006.

(31) Dewey, D. C.; Strulson, C. A.; Cacace, D. N.; Bevilacqua, P. C.; Keating, C. D. *Nat. Commun.* **2014**, *5*, 4670.

(32) Qiao, Y.; Li, M.; Booth, R.; Mann, S. *Nat. Chem.* **2017**, *9*, 110.

(33) Yang, H. Q.; Fu, L. M.; Wei, L. J.; Liang, J. F.; Binks, B. P. *J. Am. Chem. Soc.* **2015**, *137*, 1362.

(34) Zhang, M.; Wei, L. J.; Chen, H.; Du, Z. P.; Binks, B. P.; Yang, H. Q. *J. Am. Chem. Soc.* **2016**, *138*, 10173.

(35) Lach, S.; Yoon, S. M.; Grzybowski, B. A. *Chem. Soc. Rev.* **2016**, *45*, 4766.

(36) Sugiura, H.; Ito, M.; Okuaki, T.; Mori, Y.; Kitahata, H.; Takinoue, M. *Nat. Commun.* **2016**, *7*, 10212.

(37) de Oliveira, L. R.; Bazzani, A.; Glampieri, E.; Castellani, G. C. *J. Chem. Phys.* **2014**, *141*, 065102.

(38) Hallett, J. P.; Welton, T. *Chem. Rev.* **2011**, *111*, 3508.

(39) Crespy, D.; Landfester, K. *Soft Matter* **2011**, *7*, 11054.

(40) Binks, B. P.; Dyab, A. K. F.; Fletcher, P. D. I. *Chem. Commun.* **2003**, 2540.

(41) Binks, B. P.; Dyab, A. K. F.; Fletcher, P. D. I. *Phys. Chem. Chem. Phys.* **2007**, *9*, 6391.

(42) Aveyard, R.; Binks, B. P.; Clint, J. H. *Adv. Colloid Interface Sci.* **2003**, *100–102*, 503.

(43) Read, E. S.; Fujii, S.; Amalvy, J. I.; Randall, D. P.; Armes, S. P. *Langmuir* **2004**, *20*, 7422.

(44) Bradley, L. C.; Stebe, K. J.; Lee, D. *J. Am. Chem. Soc.* **2016**, *138*, 11437.

(45) Frelichowska, J.; Bolzinger, M. A.; Chevalier, Y. *Colloid Interface Sci.* **2010**, *351*, 348.

(46) van Rantwijk, F.; Sheldon, R. A. *Chem. Rev.* **2007**, *107*, 2757.

(47) Zhang, S. G.; Zhang, J. H.; Zhang, Y.; Deng, Y. Q. *Chem. Rev.* **2017**, *117*, 6755.

(48) Wang, Z. P.; van Oers, M. C. M.; Rutjes, F. P. J. T.; van Hest, J. C. M. *Angew. Chem., Int. Ed.* **2012**, *51*, 10746.

(49) Verho, O.; Bäckvall, J. E. *J. Am. Chem. Soc.* **2015**, *137*, 3996.

(50) Pushpanath, A.; Siirola, E.; Bornadel, A.; Woodlock, D.; Schell, U. *ACS Catal.* **2017**, *7*, 3204.

(51) Adamo, A.; Beingessner, R. L.; Behnam, M.; Chen, J.; Jamison, T. F.; Jensen, K. F.; Monbaliu, J. C. M.; Myerson, A. S.; Revalor, E. M.; Snead, D. R.; Stelzer, T.; Weeranoppanant, N.; Wong, S. Y.; Zhang, P. *Science* **2016**, *352*, 61.

(52) Tsubogo, T.; Oyamada, H.; Kobayashi, S. *Nature* **2015**, *520*, 329.

(53) Hefez, A. M.; Taggi, A. E.; Dudding, T.; Lectka, T. *J. Am. Chem. Soc.* **2001**, *123*, 10853.

(54) Valera, F. E.; Quaranta, M.; Moran, A.; Blacker, J.; Armstrong, A.; Cabral, J. T.; Blackmond, D. G. Angew. Chem., Int. Ed. 2010, 49, 2478.

(55) Mannel, D. S.; Ahmed, M. S.; Root, T. W.; Stahl, S. S. *J. Am. Chem. Soc.* **2017**, *139*, 1690.

(56) Li, B. Y.; Leng, K. Y.; Zhang, Y. M.; Dynes, J. J.; Wang, J.; Hu, Y. F.; Ma, D, X.; Shi, Z.; Zhu, L. K.; Zhang, D. L.; Sun, Y. Y.; Chrzanowski, M.; Ma, S. Q. *J. Am. Chem. Soc.* **2015**, *137*, 4243.

(57) Britton, J.; Meneghini, L. M.; Raston, C. L.; Weiss, G. A. *Angew. Chem., Int. Ed.* **2016**, *55*, 11387.

(58) Yao, W. H.; Wang, H. Y.; Cui, G. K.; Li, Z. Y.; Zhu, A. L.; Zhang, S. J.; Wang, J. J. *Angew. Chem., Int. Ed.* **2016**, *55*, 7934.

(59) Ali, A. A.; Konwar, M.; Chetia, M.; Sarma, D. *Tetrahedron Lett.* **2016**, *57*, 5661.

TOC: